The Nonlinear Landau-Lifshitz Equation: Ferromagnetic Resonance, Giant Magnetoimpedance, and Related Effects

D. Seddaoui, S. Loranger, M. Malatek, D. Ménard, and A. Yelon, *Life Fellow, IEEE*

Department of Engineering Physics, École Polytechnique de Montréal and Regroupement Québécois des Matériaux de Pointe (RQMP), Montréal, QC H3C 3A7, Canada

We review recent work in which a methodology has been developed for solving the Landau-Lifshitz equation in its most general form, along with Maxwell's equations. The method has been applied to the solution of problems of giant magnetoimpedance and ferromagnetic resonance. Conditions for chaotic behavior have been explored. Perspectives for future applications are briefly discussed.

***Index Terms*—Chaotic behavior, ferromagnetic resonance, giant magnetoimpedance, Landau-Lifshitz equation, nonlinear.**

I. Introduction

THE existence of ferromagnetic resonance (FMR) was first reported in 1946 [1], and the linearized Landau-Lifshitz (LL) equation was immediately applied to explaining and modelling of FMR [2]. In the 1950s, the methodology of simultaneously solving Maxwell's (M) equations and the LL equation, and satisfying the appropriate boundary conditions, was applied to FMR in metallic films [3], [4] and, in 1982, to wires [5]. The power absorbed in an FMR experiment is then obtained from the surface impedance ξ. This approach generally provides a very satisfactory account of the position of features and of linewidth in metallic wires and plates in the small ac signal regime [6] and has been extended to include various physical effects in this case [7].

More recently, the same approach has been applied to modelling of giant magnetoimpedance (GMI) [8]–[11]. For simple geometries, the passage from the FMR calculation to the calculation of bulk impedance is straightforward, since the impedance Z is given by

$$Z = \xi l/p \tag{1}$$

where l is the length of the conductor, and p is its perimeter [12]. However, most GMI experiments are performed in nonlinear conditions. Further, for sensor applications we need to maximize $\partial Z/\partial H$, which depends upon the details of these conditions.

In order to resolve this difficulty, we have recently developed a numerical solution of the full nonlinear LL equation [13] for cylindrical conductors whose properties vary only with the radius. Extension to films and plates is not difficult. Here, we present a brief summary of the methodology, and some of the results which we have obtained in its application to various circumstances.

II. Methodology

In the GMI calculation, we assume that the sample is a long cylindrical microwire, submitted to a uniform axial dc magnetic field, and that its behavior is uniform with length, z, and circumferential angle, φ. Then, the dynamic electric $E(r,t)$ and magnetic $H(r,t)$ fields within the wire are only functions of time, t, and radial position, r. The magnetic flux within the wire may be obtained by solving the LL equation, which is nonlinear, since the interaction between the dynamic magnetization and field cannot be neglected. We consider an effective field dominated by the circumferential excitation field produced by the current, including a static axial field, the anisotropy field, the demagnetizing field, and an exchange field. Since the magnetic field is not homogeneous in the wire, the M equations including Ohm's law need to be solved as well. Boundary conditions on the magnetization are required, in addition to the usual conditions on electromagnetic fields.

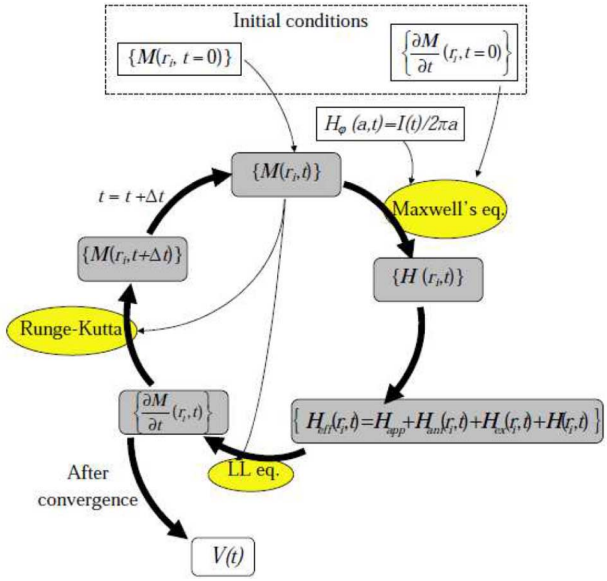

Fig. 1. Schematic representing the method used in the calculation. After [13].

The calculation [13] is summarized in Fig. 1. At $t = 0$, the magnetization of the wire is set in a static configuration. At $t > 0$, a sinusoidal current begins to flow in the wire, leading to change in the magnetization. The response time of the magnetization is very long in comparison with the time step of the calculation, Δt (of the order of 1 ps). This allows us to assume that $(\partial \boldsymbol{M})/(\partial t)(r,t)$ remains approximately constant from instant t until $t + \Delta t$. Hence, $(\partial \boldsymbol{M})/(\partial t)(r,t)$ calculated from the LL equation for instant t may be used in the M equations for instant $t + \Delta t$. This yields the dynamic magnetic field $\boldsymbol{H}(r,t)$

Manuscript received September 09, 2010; accepted September 30, 2010. Date of current version January 26, 2011. Corresponding author: D. Seddaoui (e-mail: djamel.seddaoui@polymtl.ca).

Color versions of one or more of the figures in this paper are available online at http://ieeexplore.ieee.org.

Digital Object Identifier 10.1109/TMAG.2010.2089611

TABLE I
PARAMETERS OF THE CALCULATION

σ	H_k	M_s	A	$\gamma/2\pi$	a
$8\text{x}10^5(\Omega\text{m})^{-1}$	40 A/m (0.5 Oe)	660 kA/m 0.825 T	10^{-11}J/m	28GHz/T	0.01

for instant $t+\Delta t$ which is then used in the LL equation for the same instant, and so on. The magnetization $\boldsymbol{M}(r,t+\Delta t)$ at the instant $t+\Delta t$ is calculated from $M(r,t)$ using the Runge-Kutta method. After several periods of the current, the system reaches a stationary state. Convergence is achieved when the magnetization shows periodic behavior $M(r,t+T)=M(r,t)$, where T is the current period. After convergence, when the stationary state is reached within the wire, $E_z(r,t)$ is given by [13]:

$$E_z(r,t)=\frac{R_{\rm DC}I(t)}{l}+\int_0^r\frac{\partial B_\varphi(\rho,t)}{\partial t}d\rho -\frac{2}{a^2}\int_0^a\rho\int_0^\rho\frac{\partial B_\varphi(\rho',t)}{\partial t}d\rho'\,d\rho \quad (2)$$

where $R_{\rm DC}$ is the dc resistance, l is the wire length, a is the wire radius, and $B_\varphi=\mu_0(H_\varphi+M_\varphi)$ is the circumferential induction. The voltage across the wire is obtained from the axial electric field at the wire surface:

$$V(t)=lE_z(r=a,t). \quad (3)$$

The harmonics V_{nf} are given by the Fourier transform of $V(t)$:

$$V_{nf}=\frac{2}{T}\left|\int_0^T V(t)e^{in\omega t}dt\right|. \quad (4)$$

Application to the simplest situation, of ideal wires, with regions of uniform anisotropy and free surface spins, allows us to obtain a general view of many aspects of nonlinear behavior. The parameters of the calculation for all of the examples presented here are summarized in Table I, where σ is the conductivity of the wire, H_k is the anisotropy field, M_s is the saturation magnetization, A is the exchange constant, γ is the gyromagnetic ratio, and α is a phenomenological damping coefficient.

In the nonlinear regime, the simple skin effect is no longer obtained. Instead, the calculation predicts solitary-wave-like propagation of the magnetization at fairly high current amplitude. An example of this is shown in Fig. 2, and other examples are presented in [13].

As a result, at high amplitudes, the voltage is dominated by the second term on the RHS of (2), which is maximum at zero static field. This is illustrated in Fig. 3, where we also see that the maximum slope of the MI curve is obtained in a regime of current only slightly higher than the threshold for nonlinear behavior (3 $\text{mA}_{\rm rms}$ for the parameters of the figure).

It is well known [11], [14], [15] that experimentally observed GMI curves and their slopes are smaller than expected from the linear calculation, assuming unpinned surface spins, or even a surface anisotropy. The nonlinear calculation [13] confirms this. Excellent fits to the total signal over a large range of frequency and of ac current, for a 35 μm cobalt rich amorphous microwire, were obtained assuming a hard surface layer of 6% of the radius. Even harmonics of GMI signal are very sensitive

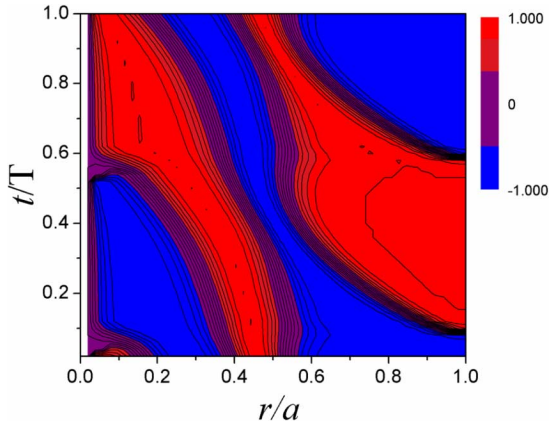

Fig. 2. Time and radial dependence of the normalized transverse component of the magnetization M_t/M_s at 10 MHz frequency and 15 $\text{mA}_{\rm rms}$ amplitude of the current. The wire diameter is 20 μm. The anisotropy is circumferential, with $H_k=40$ A/m (0.5 Oe).

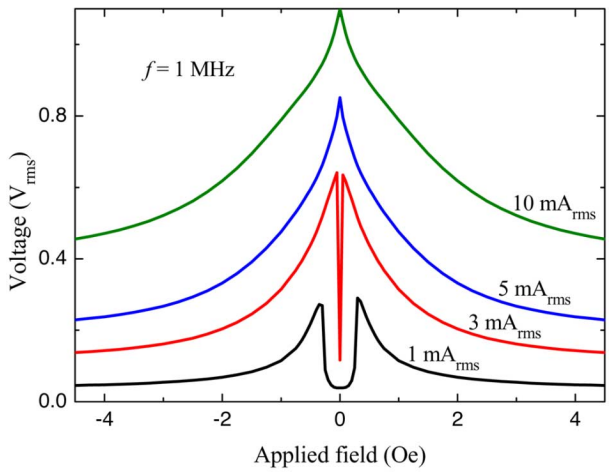

Fig. 3. Static field dependence of voltage across a 2.5 cm wire for various currents of 1 MHz frequency, and wire length 3 cm. $1Oe=10^3/4\pi$ A/m.

to the domain structure of the wire whereas the odd harmonics are not. Without changing the total signal in a significant way, the second harmonic could be fit reasonably well, assuming that the hard layer consisted of domains, equally following the two directions along the easy axis, slightly off circumferential.

We have recently attempted to reduce the hard layer by electropolishing wires from the same source. This does not appear to seriously modify the total nonlinear GMI signal observed. This may be attributed to several possible causes. The effective blocking may be due to an effect, such as nonuniform radius, which is not altered by electropolishing. It may be due to an effect, such as oxidation of the surface, which is re-established before any measurement can be made. Or, it may be due to a bulk, rather than a surface, effect. We are pursuing this investigation.

III. CHAOTIC BEHAVIOR

The results described above are for the steady state, which is the criterion for convergence presented in the discussion of methodology. We have encountered circumstances for which this criterion is never fulfilled, and verified that this is not due to computational difficulties. Under conditions of low static field, and large ac current and field, the calculations predict bifurcation, and finally, chaotic behavior.

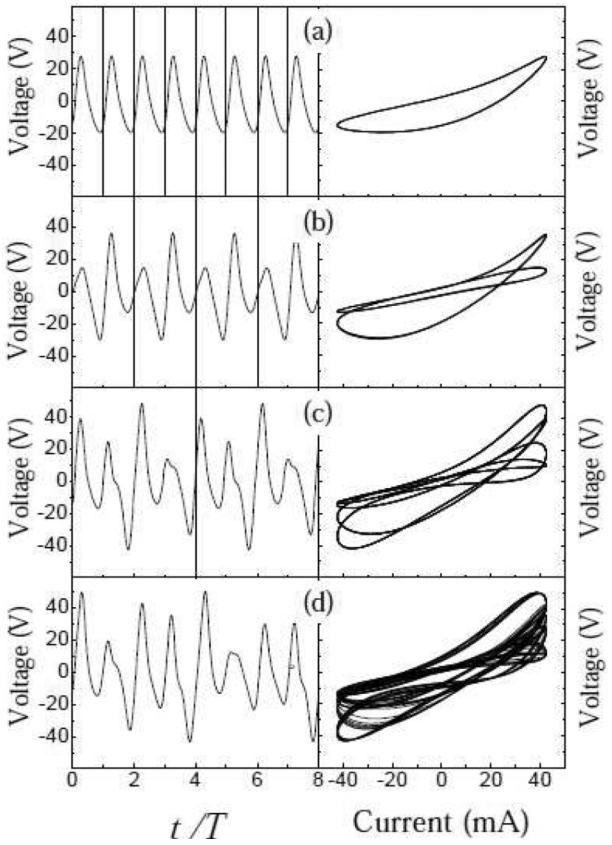

Fig. 4. Time (left-hand graphs) and current (right-hand graphs) dependence of the voltage across a 3 cm wire, for current of 30 $\mathrm{mA_{rms}}$ amplitude and 500 MHz frequency. The applied field Hz is (a) 0.7 Oe, (b) 0.6 Oe, (c) 0.4 Oe, and (d) 0.3 Oe ($1\ \mathrm{Oe} = 10^3/4\pi$ A/m). The anisotropy is transverse with $H_k = 40$ A/m (0.5 Oe). The vertical dashed lines in the left hand graphs indicate the voltage period.

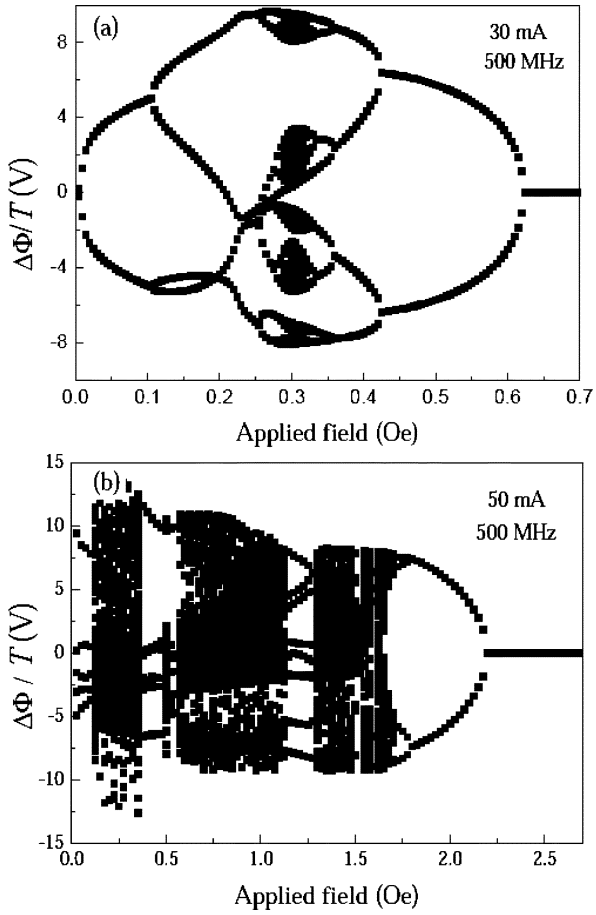

Fig. 5. Difference of circumferential magnetic flux between successive periods as a function of applied field at 500 MHz frequency and (a) 30 and (b) 50 $\mathrm{mA_{rms}}$ amplitude of current. $1\ \mathrm{Oe} = 10^3/4\pi$ A/m.

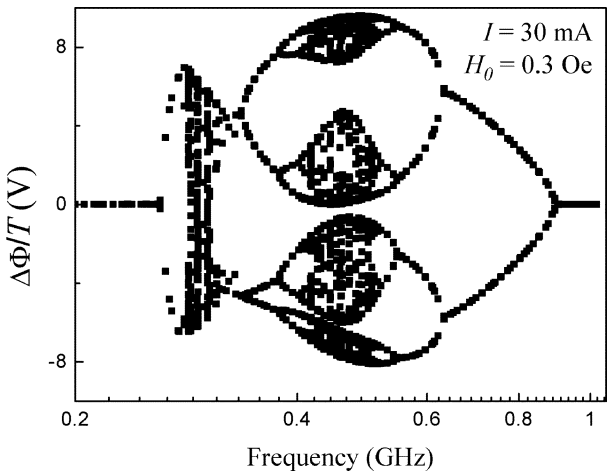

Fig. 6. Difference of circumferential magnetic flux between successive periods as a function of frequency for current of 30 $\mathrm{mA_{rms}}$ at $H_z = 24$ A/m (0.3 Oe).

In Fig. 4, we show voltage as a function of time and of current for a wire ($r = 15\ \mu$m) with free surface spins, and with an anisotropy field of 0.5 Oe, subjected to an ac current of 30 mA amplitude and a frequency of 500 Mz, for four values of static field. As the field is decreased, the voltage, initially distorted but periodic, exhibits a doubling, and then, a second doubling of the period, and finally, chaotic behavior. A convenient way of exhibiting this evolution is to present the change of flux, $\Delta\Phi$, from the beginning to the end of a period of current, which is, of course, zero in steady state. In Fig. 5, we show $\Delta\Phi$ as a function of applied field at 500 MHz, for a 30 mA current, which produces a maximum surface field on the wire of 4 Oe, and a 50 mA current, which produces a 6.6 Oe field. As expected, the higher current results in increased chaotic behavior, but always over several separated ranges of field (interlaced with windows of order). In Fig. 6, we show $\Delta\Phi$ as a function of frequency, for fixed current, 30 mA, and static field, 0.3 Oe. There is a minimum frequency, below which there is no bifurcation, and a maximum frequency, above which there is no bifurcation. Again, there are disconnected ranges of frequency in which chaotic behavior occurs.

We have not yet found a simple explanation for the details of this behavior, but we have found a curious correlation with FMR. Fig. 7 shows the frequencies at which chaotic behavior is predicted as a function of static field, for three values of current. In the figure, f_r is the FMR frequency of the wire, and f_{r0} is the FMR frequency calculated when exchange is neglected. We note, first, that the lowest frequency for chaotic behavior is slightly above f_r. Second, we note that chaos is first observed at fields and frequencies for which integral multiples of the two intersect. Finally, as current increases, the region of chaotic behavior appears to extend following the two types of curves. We continue to pursue this problem.

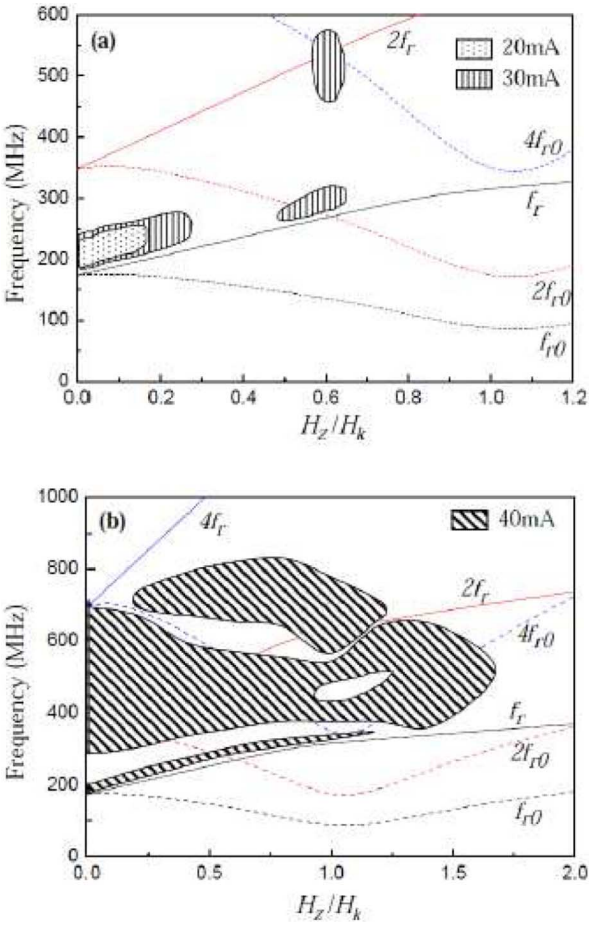

Fig. 7. Conditions of chaotic behavior for currents (a) 20 and 30 $\mathrm{mA_{rms}}$ and (b) 40 $\mathrm{mA_{rms}}$.

IV. FMR at Low Effective Field and Frequency

While the precession of M near FMR may be very distorted in the nonlinear regime, f_r at high field and frequency is essentially indistinguishable from the value predicted by the linearized LL equation. We have recently found [16] that this is not the case at low effective field and frequency. Let us consider an ideal case: a monodomain, uniaxial, ferromagnetic thin film subjected to static longitudinal and sinusoidal transverse in-plan magnetic fields, with the easy axis exactly or nearly transverse, as shown in Fig. 8. For exactly transverse anisotropy, $(\psi = 0)$, the linear approximation predicts that the ferromagnetic resonance frequency is given by

$$f_r = \mu_0|\gamma|\sqrt{\frac{(M_s + H_z)}{H_k}\,(H_k^2 - H_z^2)} \quad \text{for } H_z \le H_k \quad (5a)$$

and

$$f_r = \mu_0|\gamma|\sqrt{(M_s + H_z)(H_z - H_k)} \quad \text{for } H_z \ge H_k. \quad (5b)$$

In (5), μ_0 is the permeability of free space, and γ is the gyromagnetic ratio. We may easily see that (5) predicts that f_r goes to zero when the longitudinal field is equal to the anisotropy field, that is, when the static effective field goes to zero, as shown in Fig. 9. Fig. 10 shows the resonance frequency f_r as determined

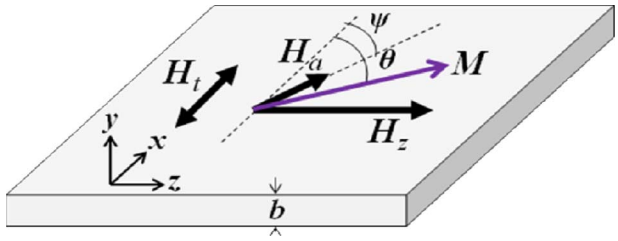

Fig. 8. Schematic of thin film subjected to a static magnetic field H_z parallel to z axis and an ac field H_t transverse to H_z. After [16].

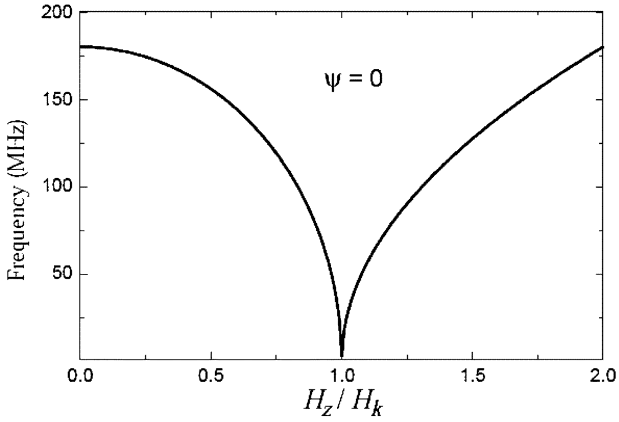

Fig. 9. Resonance condition in the linear approximation for exactly transverse anisotropy.

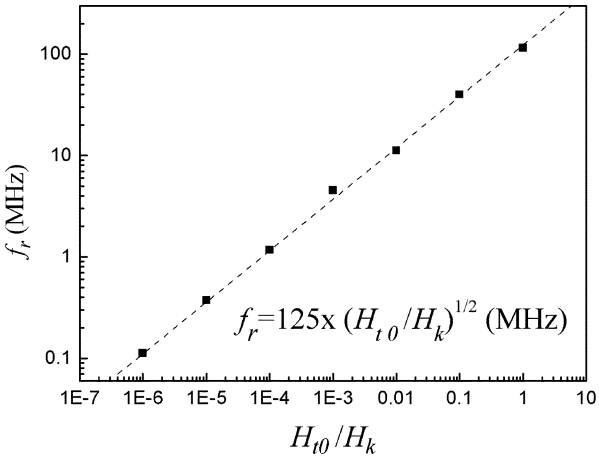

Fig. 10. Resonance frequency calculated numerically as a function of the normalized amplitude of the transverse field. After [16].

from $X(f) = 0$ (where X is the imaginary part of ξ), as a function of H_{t0}/H_k at $H_z = H_k$. A linear fit of the curve of Fig. 10 gives

$$f_r = C\sqrt{H_{t0}/H_k} \quad (6)$$

where C is a constant [16] and H_{t0} is the amplitude of the transverse ac field. Thus, $f_r = 0$ at $H_z = H_k$ only for $H_{t0} = 0$, in contrast with the prediction of the linearized calculation. In fact, at low resonance frequency, the resonance field is less than the anisotropy field. This shift increases as the ac field is increased.

Fig. 11 shows the calculated FMR versus H_z plots for $H_{t0} = 0.2\ H_k$, H_k, and $2H_k$ for $\psi = 0$. Interesting changes are also predicted for small nonzero values of ψ. Fig. 12 shows the prediction for $\psi = 2°$, and $H_{t0} = 0.2\ H_k$. We note that the upper

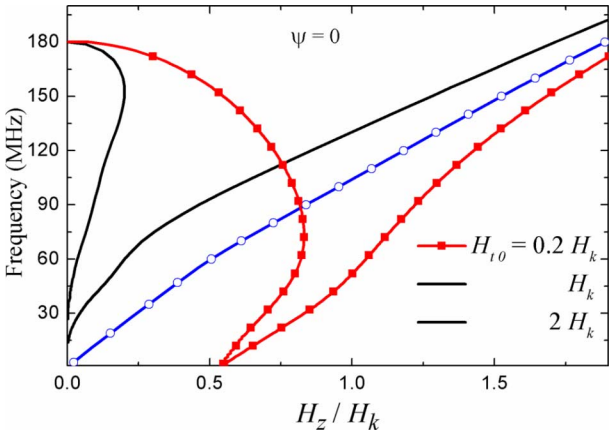

Fig. 11. Resonance conditions $(X = 0)$ for different values of the amplitude of the transverse ac field in the case of rigorously transverse anisotropy.

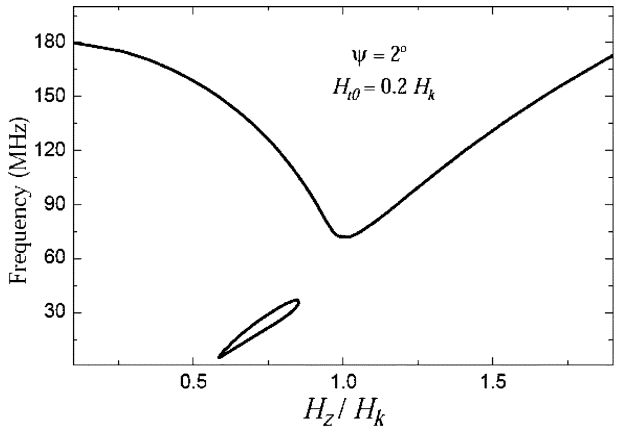

Fig. 12. Resonance conditions $(X = 0)$ for $H_{t0} = 0.2\ H_k$ with $\psi = 2°$.

branch of this curve is very close to the prediction of the linearized equation for frequencies above about 100 MHz, and that the curves of Fig. 11 are very close above about 200 MHz. The difference between the linear and nonlinear values of resonance frequency for a given static field is explained in terms of switching times shorter than the period at low frequency [16]. Similar effects are to be expected for other situations in which the internal static field is close to zero, and similar conditions should apply to microwave generation by spin transfer torque at low fields [17].

V. Conclusion

We have briefly described the methodology for calculating the electromagnetic behavior of ferromagnetic samples with general metallic and dielectric properties, subjected to ac currents or fields of arbitrary amplitudes, but with certain simplifications of their geometries. We have presented three applications of this methodology: nonlinear GMI in wires, chaotic behavior, and FMR at very low field and frequency. This is far from all of the possible subjects which can be investigated using the approach described here. For example, the same methodology is applicable to problems such as parallel pumping.

The analogous methodology, in which the equation of motion is the linearized LL equation [3], [4], has been widely applied, taking account of many properties of ferromagnets and of sample geometries [7]. It continues to be used more than 55 years after its development. We believe that the extension to nonlinear behavior should likewise be widely useful. In order to permit this, the program for these calculations is available from the corresponding author.

Acknowledgment

This work was supported by a Collaborative Research and Development grant from the Natural Sciences and Engineering Research Council of Canada (NSERC) and Custom Security Industries (CSI). Morton Roseman, of CSI, has aided and encouraged progress in this program.

References

[1] J. H. E. Griffiths, "Anomalous high frequency resistance of ferromagnetic metals," *Nature*, vol. 158, pp. 670–671, 1946.
[2] S. V. Vonsovskii, *Ferromagnetic Resonance*. Jerusalem: Israel Program for Scientific Translations, 1964.
[3] J. R. MacDonald, "Spin exchange effects in ferromagnetic resonance," *Phys. Rev.*, vol. 103, pp. 280–286, 1956.
[4] W. S. Ament and G. T. Rado, "Electromagnetic effects of spin wave resonance in ferromagnetic metals," *Phys. Rev.*, vol. 97, pp. 1558–1566, 1955.
[5] L. Kraus, "Theory of ferromagnetic resonances in wires," *Czech J. Phys. B*, vol. 32, pp. 1264–1282, 1982.
[6] A. G. Gurevich and G. A. Melkov, *Magnetization Oscillations and Waves*. Boca Raton, FL: CRC, 1996.
[7] P. Ciureanu, L. G. C. Melo, D. Seddaoui, D. Ménard, and A. Yelon, "Physical models of magnetoimpedance," *J. Appl. Phys.*, vol. 102, pp. 073908 1–073908 8, 2007.
[8] D. Ménard, M. Britel, P. Ciureanu, and A. Yelon, "Giant magnetoimpedance in a cylindrical magnetic conductor," *J. Appl. Phys.*, vol. 84, pp. 2805–2814, 1998.
[9] D. Menard and A. Yelon, "Theory of longitudinal magnetoimpedance in wires," *J. Appl. Phys.*, vol. 88, pp. 379–393, 2000.
[10] L. Kraus, "Theory of magneto-impedance in the planar conductor with uniaxial magnetic anisotropy," *J. Magn. Magn. Mater.*, vol. 195, pp. 764–778, 1999.
[11] M. Knobel, M. Vázquez, and L. Kraus, *Handbook of Magnetic Materials 15*, K. H. J. Buschow, Ed. London, U.K.: Elsevier, 2003, p. 497.
[12] A. Yelon, D. Ménard, M. Britel, and P. Ciureanu, "Calculations of giant magnetoimpedance and of ferromagnetic resonance response are rigorously equivalent," *Appl. Phys. Lett.*, vol. 69, pp. 3084–3085, 1996.
[13] D. Seddaoui, D. Ménard, B. Movaghar, and A. Yelon, "Nonlinear electromagnetic response of ferromagnetic metals: Magnetoimpedance in microwires," *J. Appl. Phys.*, vol. 105, p. 063916, 2009.
[14] L. Kraus, "The theoretical limits of giant maneto-impedance," *J. Magn. Magn. Mater.*, vol. 196–197, pp. 354–356, 1999.
[15] L. G. C. Melo, D. Ménard, P. Ciureanu, and A. Yelon, "Influence of surface anisotropy on magnetoimpedance in wires," *J. Appl. Phys.*, vol. 92, pp. 7272–7280, 2002.
[16] D. Seddaoui, S. Loranger, D. Ménard, and A. Yelon, "The Landau-Lifshitz equation for magnetization dynamics of thin films: Failure of the linear approximation at low effective field," *Phys. Rev. B*, vol. 82, p. 134430, 2010.
[17] O. Boulle, V. Cros, J. Grollier, L. G. Pereira, C. Deranlot, F. Petroff, G. Fain, J. Barnas, and A. Fert, "Shaped angular dependence of the spin-transfer torque and microwave generation without magnetic field," *Nature Phys.*, vol. 3, pp. 492–497, 2007.